RSC Advances

PAPER

View Article Online
View Journal | View Issue

Cite this: *RSC Adv.*, 2022, **12**, 5587

Efficient adsorption of methyl orange and methyl blue dyes by a novel triptycene-based hyper-crosslinked porous polymer†

Yan He, *[ab] Wenli Bao,[a] Yingcen Hua,[a] Zhulei Guo,[a] Xiaolei Fu,[a] Bing Na,[a] Dingzhong Yuan,[a] Changjun Peng *[b] and Honglai Liu[b]

Received 23rd November 2021
Accepted 14th January 2022

DOI: 10.1039/d1ra08589a

rsc.li/rsc-advances

It is still a great challenge to develop new materials for the highly efficient entrapment of organic dyes from aqueous solution. Herein, a novel triptycene-based hyper-crosslinked porous polymer (TPP–PP) was designed and synthesized by a simple Friedel–Crafts reaction. The obtained polymer TPP–PP has a high surface area, abundant pore structure and stable thermal performance. Due to the above characteristics, TPP–PP has good adsorption performance for anionic methyl orange solution (MO) and cationic methyl blue solution (MB). Under the optimal experiment conditions, the TPP–PP showed an excellent adsorption capacity for MO (220.82 mg g^{-1}) and MB (159.80 mg g^{-1}), respectively. The adsorption kinetics fitted the pseudo-second-order model. The adsorption of MO by TPP–PP reaches equilibrium within 180 minutes, and the adsorption of MB reaches equilibrium within 150 minutes. The adsorption behavior was not only spontaneous but also endothermic in reality. At the same time, TPP–PP also has good reusability. After 5 cycles of experiments, the removal rate of MO and MB by TPP–PP can still reach more than 80%. Thus, the Friedel–Crafts reaction crosslinked method might be a promising approach for the synthesis of novel material for the highly efficient extraction of dye wastewater.

1. Introduction

With the rapid development of the printing and dyeing industry, dye wastewater has become an important source of water pollution.[1] Dye wastewater contains a large number of chemicals hazardous to the human body and the environment,[2] such as methyl orange, methyl blue, and Congo red. Thus, how to rapidly and efficiently remove dye from wastewater has become an urgent environmental issue. A variety of methods such as photocatalytic degradation,[3] biological degradation,[4] electrochemical oxidation[5] and adsorption[6] has been systematically investigated to remove dye from wastewater. Among these methods, adsorption by porous materials is regarded as a promising approach owing to its economic viability, high efficiency, and tolerance to pH change.[7] Many adsorbents, such as activated carbon,[8] zeolites,[9] coated silica gel,[10] and activated alumina,[11] have been developed for removing dyes from polluted wastewater. However, the obvious shortcoming of traditional porous adsorption materials is low adsorption capacity and the necessity for a multi-step synthesis of these porous polymers may potentially limit their further applications. Therefore, exploring novel porous adsorbents for efficient adsorption and removal of dyes is still of current mainstream direction.[12]

Porous organic polymers (POPs),[13] a novel type of porous materials have been widely used in catalysis,[14] gas storage and separation,[15] adsorption, sensor technology,[16] and energy storage and conversion[17] owing to their large specific surface area, low skeleton density, diverse structures, and good thermal stability. In the last several years, researchers have made great efforts to enhance the adsorption capacity of the POP frameworks toward organic dyes *via* rational design.[18–20] For example, the saturation magnetization of the POPs is tunable by controlling the number of magnetic nanoparticles during the reaction process,[21] the as-synthesized POPs presented ultrahigh adsorption capacities. However, the expensive monomers, rare metal catalysts used and multiple synthetic steps limit their large-scale applications. Recently, Tan and co-workers successfully developed a low-cost synthetic method for hyper-crosslinked porous polymers (HCPs).[22] The aromatic benzene, biphenyl, phenol, triphenyl and other monomers can be polymerized into porous materials through one-step of simple Friedel–Crafts alkylation using formaldehyde dimethyl acetal (FDA) as an external cross-linker. This provides new ideas and directions for subsequent development.

[a]*Jiangxi Province Key Laboratory of Polymer Micro/Nano Manufacturing and Devices, School of Chemistry, Biology and Materials Science, East China University of Technology, Nanchang, 330013, China*

[b]*Key Laboratory for Advanced Materials, Department of Chemistry, East China University of Science and Technology, Shanghai, 200237, China*

† Electronic supplementary information (ESI) available. See DOI: 10.1039/d1ra08589a

As known, organic dye molecules usually have good planar conjugated structures together with specific polar functional groups. For improving the adsorption rate toward organic dyes, the structure of the HCP material was rationally designed.[23] Herein, we selected monomers the one is three dimensional (3D) rigid structure triptycene which may increase the dye affinity by means of the π–π interactions and the other is nitrogen-doped structure pyrrole which may increase the dye affinity by means of the electrostatic interactions. Then in the presence of cross-linker FDA and Lewis acid $FeCl_3$, the above monomers were cross-linked by a simple Friedel–Crafts reaction to obtain a novel triptycene-based hyper-crosslinked porous polymer (TPP–PP). The obtained polymer was found to exhibit good adsorption for MO and MB. Subsequently, a series of adsorption experiments were carried out, including adsorption isotherms and kinetics, the effect of pH and regeneration of adsorbent *etc.* And the adsorption effect was compared with triptycene porous polymer (TPP) and the pyrrole porous polymer (PP). These results show that TPP–PP can become a new and efficient adsorbent for dye wastewater treatment.

2. Experimental part

2.1. Reagents

All reagents used are commercially available and the purity of reagents is AR. Methyl orange, methyl blue, triptycene (98%), nitric acid (65%), sodium carbonate, 1,2-dichloroethane (99%), anhydrous methanol (99.5%), benzaldehyde dimethyl acetal (98%), pyrrole (99%), anhydrous ferric chloride (98%) were purchased from Aladdin Reagent Co., Ltd.

2.2. Synthesis of triptycene-based hyper-crosslinked porous polymer TPP–PP

As shown in Fig. 1, place the monomer triptycene (4 mmol, 1.0088 g) and pyrrole (4 mmol, 0.2775 mL) in a round bottom flask, and then add 1,2-dichloroethane (20 mL) to dissolve the monomers. Formaldehyde dimethyl acetal (FDA, 16 mmol) and anhydrous $FeCl_3$ (16 mmol) were added sequentially to an experimental round bottom flask under nitrogen atmosphere. And after thorough mixing the mixture was heated to 80 °C in an oil bath and then the reaction was continued with magnetic stirring for 24 hours. After the reaction is over, cool to room temperature, collect the crude product by filtration, and wash with methanol for several times until the filtrate is almost colorless. Then, the filtered crude product was purified by Soxhlet extraction with methanol for 24 hours, and after Soxhlet extraction, it was vacuum dried at 80 °C for 12 hours to obtain powder TPP–PP (yield: 98.4%).

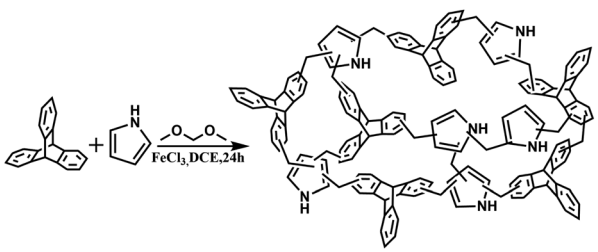

Fig. 1 The schematic representation of triptycene-based hyper-crosslinked porous polymer TPP–PP.

Similarly, we used the same method to synthesize the polymer TPP and PP, and the detailed description of the synthesis procedure was described in the ESI.†

2.3. Characterization

A polycrystalline X-ray diffractometer (D8 advance; Bruker, Germany) was used to analyze the crystalline properties of the sample. The voltage of the Cu target X-ray tube was ≤40 kV, and the current was ≤40 mA. A Zeiss Sigma 300 field emission scanning electron microscope (SEM) was used to characterize the morphology of the sample powder. A transmission electron microscope (JEOL JEM-2100) TEM was used to record the transmission image of the material. A Fourier infrared spectrometer (Nicolet5700) was used to analysis and record infrared spectral data. A thermogravimetric analyzer (NETTZSCH STA 499) was used to characterize the thermal stability of the material.

2.4. Adsorption experiment

2.4.1. The influence of pH on the adsorption performance of TPP–PP. In this work, the adsorption effects of TPP–PP on the adsorption of methyl orange solution (MO) and methyl blue solution (MB) were studied separately at different pH values. Repeatedly weigh 5 mg polymers TPP–PP, TPP, PP in a 10 mL glass sample bottle at room temperature. Then add 5 mL MO solution and MB solution respectively and adjust the pH of the solution. The pH environment required in this work is 2, 3, 4, 5, 6, 7, 8. Adsorb in a mechanical shaker for 12 hours, and set the shaker temperature at 25 °C. After the reaction, the reaction solution was filtered with a 10 mL disposable syringe and 0.22 μm microporous PTFE membrane. A dual-beam UV-vis spectrophotometer was used to measure the absorbance of the solution after adsorption and calculate the concentration of MO and MD in the filtrate. In order to reduce the experimental error, three parallel experiments were set up for all experiments.

2.4.2. Study on adsorption isotherms of TPP–PP, TPP and PP on MO and MB. In this work, the adsorption properties of TPP–PP, TPP, and PP to methyl orange solution (MO) and methyl blue solution (MB) were studied. The adsorption performance of TPP–PP on Mo and MB was compared by using TPP and PP as a comparison. We repeatedly weighed 5 mg of TPP–P–PP copolymer TPP and PP in 10 mL glass sample bottles at room temperature, add 5 mL with a concentration gradient of 5 mg L^{-1}, 10 mg L^{-1}, 20 mg L^{-1}, 40 mg L^{-1}, 60 mg L^{-1}, 80 mg L^{-1}, 100 mg L^{-1}, 200 mg L^{-1}, 300 mg L^{-1}, 400 mg L^{-1}, 500 mg L^{-1} MO and MB solutions. Then adsorbed in a mechanical shaker for 12 hours, the shaker temperature is set at 25 °C. After the reaction, the adsorbed solution was removed by filtration using a 10 mL disposable syringe and a 0.22 μm microporous PTFE membrane. In order to reduce the experimental error, three parallel experiments were set up for all experiments. The maximum absorbance of the adsorbed

solution was measured using a double-beam UV spectrophotometer and the concentration of MO and MB in the filtrate was calculated. The adsorption capacity and removal percentage of MO and MB on TPP–PP, TPP and PP are calculated according to the following equations.[24–26]

$$q_e = \frac{(C_0 - C_e) \times v}{m} \quad (1)$$

$$E = \frac{C_0 - C_e}{C_0} \times 100\% \quad (2)$$

where q_e is the adsorption capacity when the adsorption has reached equilibrium (mg g^{-1}); C_0 is the initial concentration of MO and MB solution before adsorption; C_e is the equilibrium concentration of MO and MB solution after adsorption; V is the volume of MO and MB solution used in the experiment (mL); m is the mass (mg) of copolymers TPP–PP, TPP and PP; E is the removal percentage of MO and MB.

2.4.3. Thermodynamic study of TPP–PP, TPP, PP on MO and MB. The effects of TPP–PP, TPP and PP on the adsorption performance of methyl orange solution (MO) and methyl blue solution (MB) under different temperature conditions were studied. Repeatedly weigh 5 mg copolymers TPP–PP, TPP and PP at room temperature and place them in a 10 mL glass sample bottle, and add 5 mL of MO and MB solution with a concentration of 40 mg L^{-1}. Then it was adsorbed on a mechanical shaker for 12 hours, and the shaker temperature was set at 25 °C, 35 °C, and 45 °C. After the reaction, the reaction solution was filtered with a 10 mL disposable syringe and 0.22 μm microporous PTFE membrane. A dual-beam UV-vis spectrophotometer was used to measure the absorbance of the solution after adsorption and calculate the concentration of MO and MB in the filtrate. In order to reduce the experimental error, three parallel experiments were set up for all experiments.

2.4.4. Study on the kinetics of TPP–PP, TPP and PP on MO and MB. In this work, the effects of TPP–PP, TPP, and PP on the adsorption of methyl orange solution (MO) and methyl blue solution (MB) under different adsorption reaction times were studied. Repeatedly weigh 5 mg of copolymers TPP–PP, TPP, and PP at room temperature and place them in a 10 mL glass sample bottle, and add 5 mL of 300 mg L^{-1} MO solution and MB solution respectively. The adsorption time in the mechanical shaker is 10 min, 20 min, 30 min, 60 min, 90 min, 120 min, 180 min, 240 min, 300 min, 360 min. After the adsorption is completed, it is filter through a 0.22 μm microporous PTFE membrane, a dual-beam UV-vis spectrophotometer was used to measure the absorbance of the solution after adsorption and calculate the concentration of MO and MD in the filtrate. In order to reduce the experimental error, three parallel experiments were set up for all experiments.

2.4.5. Research on the reusability of TPP–PP. 50 mg of copolymer TPP–PP was added to 25 mL MO solution and MB solution with a concentration of 20 mg L^{-1}, and adsorbed on a mechanical shaker at 45 °C for 12 hours. After adsorption, the adsorbent and the MO and MB solutions were separated by centrifugation, and the supernatant was taken to measure the concentration of the adsorbed solution with a UV-vis spectrophotometer and calculate the removal rate. The remaining mixed solution was washed several times with 0.1 mol L^{-1} nitric acid, and then the adsorbent was collected by filtration, and vacuum dried at 80 °C for 6 hours. The above experimental steps were repeated 5 times. In order to reduce the experimental error, three parallel experiments were set up for all experiments.

3. Results and discussion

3.1. Characterization

This work first uses FT-IR to characterize TPP–PP, TPP, and PP materials. The infrared spectrum of the TPP–PP, TPP and PP is shown in Fig. 2(a), which is attributed to the stretching vibration of the N–H of TPP–PP and PP at the absorption peak of the 3438 cm^{-1} in Fig. 2(a). The absorption peak at 2990–3057 cm^{-1} of trichothene belongs to the C–H group stretching vibration II at the bridgehead carbon atom on TPP–PP,TPP, and PP. The peak of 1400 cm^{-1} is owing to the stretching vibration –CNC.

The thermal stability of the material is characterized as shown in Fig. 2(b). The thermal analyzer system performs thermogravimetric analysis at a heating rate of 10 °C min^{-1} in a nitrogen atmosphere. Fig. 2(b) thermogravimetric analysis shows that TPP–PP has very good thermal stability. The initial small weight loss below 500 °C is mainly due to the release of water molecules or some small gas molecules entrained in the

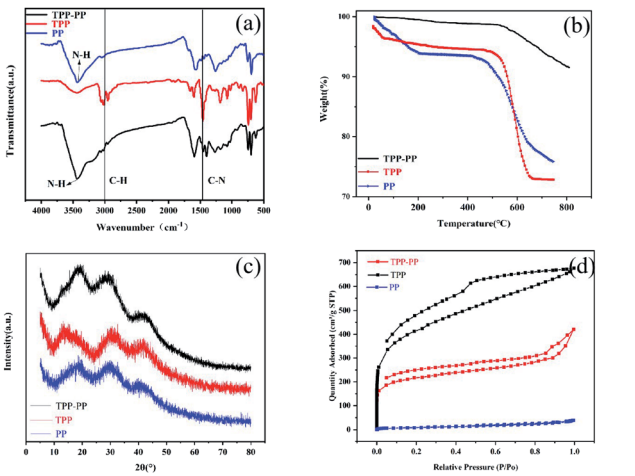

Fig. 2 (a) FT-IR spectrum of TPP–PP, TPP, PP; (b) the TG patterns of TPP–PP, TPP, PP; (c) XRD of TPP–PP TPP, PP; (d) N_2 adsorption–desorption isotherms of TPP–PP TPP, PP at 77 K.

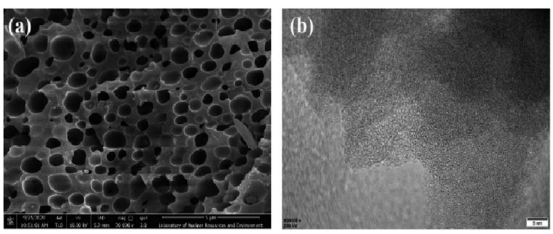

Fig. 3 (a) SEM and (b) TEM images of TPP–PP.

micropores. At 0–500 °C, the material loses less weight and is relatively stable. After the temperature reaches 500 °C, as the temperature continues to rise, the pyrrole group begins to gradually decompose. At 800 °C, TPP–PP still has a mass of more than 90%, indicating that the polymer has good thermal stability. The quality of TPP and PP materials can remain basically unchanged within 500 °C, showing good thermal stability. The mass loss at around 100 °C is the solvent molecules in the porous structure of TPP. Due to the complex internal pores, it is difficult to remove all these solvent molecules under vacuum drying.[27–29]

Through XRD analysis and observation, it was found that the diffraction peaks in the figure range from 10° to 40° in Fig. 2(c). TPP–PP have amorphous and non-crystalline properties. The BET specific surface area of TPP–PP measured from the nitrogen isotherms was 698.14 $m^2\ g^{-1}$. The initial sharp increase of uptake at low pressure ($p/p_0 < 0.1$) indicated a significant microporous character. The hysteresis loops under high pressure ($p/p_0 > 0.8$) demonstrated the existence of interarticular voids and macropores.[30]

As seen in Fig. 3, there are many irregular pore structures on the surface of TPP–PP material, and its size distribution is not uniform. The results show that it has a rich amorphous mesoporous structure. The SEM diagram and TEM diagram of TPP and PP are in the support information.

3.2. The influence of pH on the adsorption performance of TPP–PP, TPP and PP on MO and MB

Through the study of pH, it is found that when the pH value is low, the removal percentage of methyl orange and methyl blue is low. Since the chemical structure of MO and MB contains $-SO_3$ groups, the main adsorption mechanism at this time is dependent on electrostatic adsorption. Under strong acid conditions, the presence of a large amount of H^+ ions in the solution will produce strong electrostatic repulsion, preventing the contact between the dyes (MB and MO) molecules and TPP–PP. Thus, the relatively weak interaction between dyes (MB and MO) molecules and TPP–PP.[31] As the pH value increases, the electrostatic repulsion begins to be weaken.[32] The contact between TPP–PP and dyes (MB and MO) molecules gradually increases. Hence, the adsorption capacity for MB and MO increases owing to the electrostatic interaction between the N atom in the TPP–PP and SO_3 group. When the pH value is alkaline, the solution contains a large amount of OH–, it may exist the competitive adsorption with MB and MO.[33,34] When the pH value is higher 7, the adsorption capacity for MB and MO slowly decreased. So, the optimal pH value is 6 for MB and MO. And in the comparison of TPP and PP, it is found that the adsorption capacity is the best when the pH value is 6. Therefore, the pH value of the subsequent experiments is all 6 (Fig. 4).

3.3. Kinetic study of TPP–PP, TPP, PP on MO and MB

The adsorption behavior, pseudo-first-order kinetic model and pseudo-second-order kinetic model of TPP–PP, TPP, PP on MO and MB were studied in this experiment respectively. The

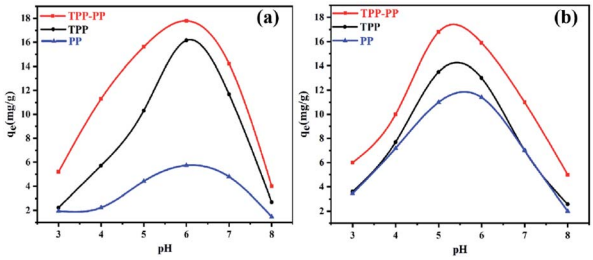

Fig. 4 The influence of pH on the adsorption effect of (a) MO and (b) MB.

equations of pseudo-first-order kinetic model and pseudo-second-order kinetic model are as follows.[35–37]

$$\ln(q_e - q_t) = \ln q_e - k_1 t \quad (3)$$

$$\frac{t}{q_t} = \frac{1}{k_2 q_e^2} + \frac{t}{q_e} \quad (4)$$

In the above equations, q_e is the equilibrium adsorption capacity; qt represents the amount of adsorptiont at a given time; k_1 is a pseudo-first-order kinetic rate constant; k_2 is a pseudo-second-order kinetic rate constant.

The kinetic study of TPP–PP found that MO needs to overcome the diffusion resistance at the beginning of the reaction and is adsorbed by some active sites.[38] As shown in Fig. 5(a) and (b), at the beginning, there are many unused active sites on the surface of the adsorbent,[39] and the adsorption reaction rate is very fast. As the adsorption time increased, the adsorption capacity gradually slowed down, and reached equilibrium due to the adsorption sites of the adsorbent gradually decrease. The optimum adsorption time is 3 hours. Also, the same trend is suited for MB adsorption on TPP–PP. It is worth mentioned that the TPP and PP also have the same trend. Then we used the

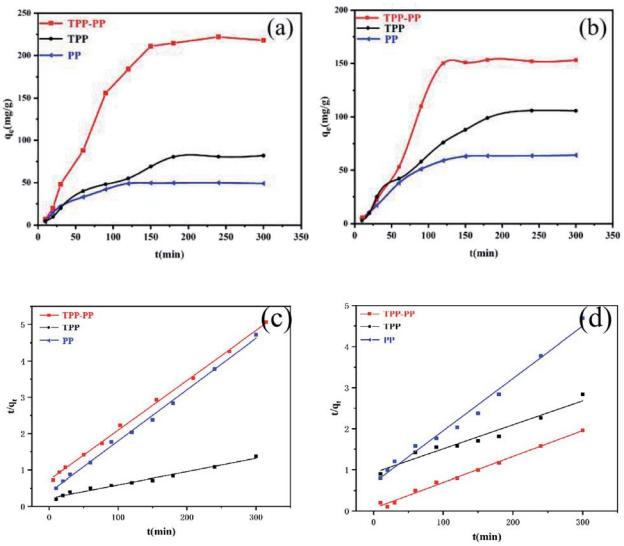

Fig. 5 (a) The adsorption kinetics curve of MO, (b) the adsorption kinetics curve of MB, (c) pseudo-second-order kinetic model of MO, (d) pseudo-second-order kinetic model of MB.

pseudo-first-order kinetic model and the pseudo-second-order kinetic model[40] to fit the experimental data. The distribution of the points fitted by the pseudo-first-order kinetic model was uneven, and the correlation coefficient R^2 was much smaller than that of the pseudo-second-order kinetic model coefficient R^2 (Fig. 5(c) and (d) and Table S1, ESI†). Therefore, the adsorption process of TPP–PP, TPP and PP on MO and MB is more in line with the pseudo-second-order kinetic model. This suggests that the rate of adsorption of the organic dyes on the TPP–PP, TPP and PP adsorbent depends on the availability of adsorption sites.

3.4. Study on the adsorption isotherms of TPP–PP, TPP, PP on MO and MB

The results of this work are fitted with Langmuir and Freundlich models.[41] The Langmuir and Freundlich equations are expressed as following.[42–44]

$$\frac{C_e}{q_e} = \frac{C_e}{q_m} + \frac{1}{K_L q_m} \quad (5)$$

$$\ln q_e = \ln K_F + \frac{1}{n} \ln C_e \quad (6)$$

q_e is the equilibrium adsorption capacity; c_e is the concentration after adsorption; K_L is the Langmuir constant; K_F is the Freundlich constant.

At different initial concentrations, the adsorption effects of TPP–PP, TPP, and PP on MO solution and MB solution are shown in Fig. 6. In the adsorption process of MO, when the concentration is low, because TPP–PP contains many adsorption sites,[45] its adsorption capacity increases rapidly. As the concentration increases, the adsorption capacity gradually tends to be flat due to the available adsorption sites gradually decrease until the saturation equilibrium. When the solution concentration is 300 mg L^{-1} and above, under the action of many pore structures, adsorption sites and adsorption groups, the maximum adsorption capacity can reach 220.82 mg g^{-1}. The experimental data were fitted with the Langmuir and Freundlich models and the results are shown in Fig. 6(c). The correlation coefficient R^2 of the Langmuir model is higher than that of the Freundlich model (Table S2, ESI†). This indicates that the experimental data fits better with the Langmuir model, which MO adsorption on polymers is monolayer adsorption. In contrast, the maximum adsorption capacity of MO for TPP and PP is only 81.63 mg g^{-1} and 50.77 mg g^{-1}, indicating that the adsorption effect of TPP–PP far exceeds that of TPP and PP materials. Similarly, in the adsorption process of MB on TPP–PP also showed a good adsorption effect. The maximum adsorption capacity of MB can reach 159.80 mg g^{-1} while the adsorption capacity of TPP and PP is 107.95 mg g^{-1} and 62.78 mg g^{-1}. Later, the Langmuir isotherm model and the Freundlich isotherm model are used to fit the experimental data as shown in Fig. 6(d). Obviously, compared with the Freundlich model, the experimental data is more consistent with the Langmuir model with a higher correlation coefficient (Table S2, ESI†), indicating that the adsorption process is a single layer adsorption.[46]

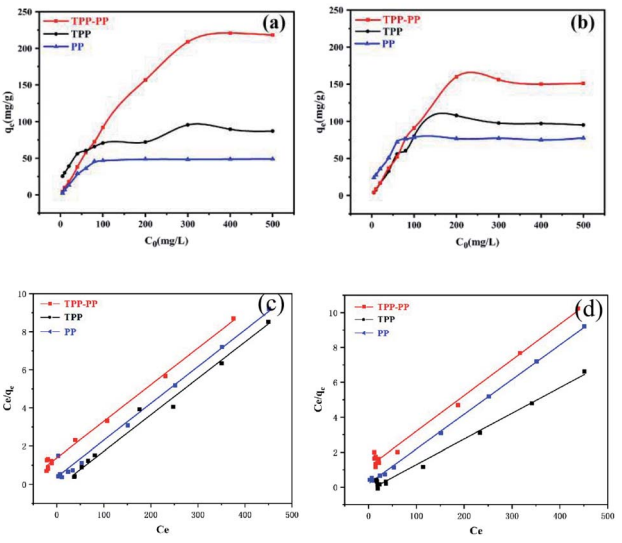

Fig. 6 (a) The relationship between the initial concentration of MO and the amount of adsorption, (b) the relationship between the initial concentration of MB and the amount of adsorption, (c) the corresponding Langmuir plots of MO, (d) the corresponding Langmuir plots of MB.

3.5. Thermodynamic study of TPP–PP, TPP, PP on MO and MB

For thermodynamic research, this work takes three temperatures of 25 °C, 35 °C, and 45 °C respectively, discusses the adsorption effects of TPP–PP, TPP, PP on MO and MB at different temperatures and calculates its thermodynamic parameters. The thermodynamic formula is as follows.[47–49]

$$\Delta G = -RT \ln K_d \quad (7)$$

$$\Delta G = \Delta H - T\Delta S \quad (8)$$

$$\ln K_d = \frac{\Delta S}{R} - \frac{\Delta H}{RT} \quad (9)$$

ΔG is the Gibbs free energy, in kJ mol; ΔH is the enthalpy change, in kJ mol; ΔS is the entropy change of the adsorption reaction, in J mol^{-1}. It can be calculated by the above formula. Where T is the temperature of the solution, the unit is K, R is the

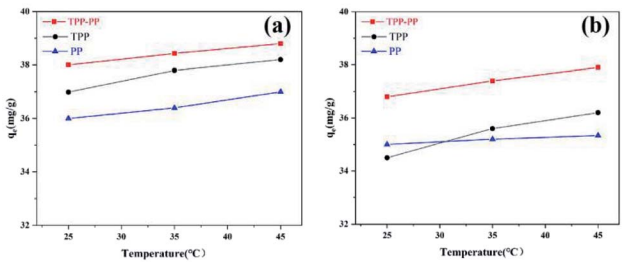

Fig. 7 (a) is the thermodynamic curve of TPP–PP, TPP, PP for MO, (b) is the thermodynamic curve of TPP–PP, TPP, PP for MB.

Table 1 Thermodynamic parameters of TPP–PP adsorption to methyl orange

Temperature (K)	ΔG (kJ mol^{-1})	ΔH (kJ mol^{-1})	ΔS (J mol^{-1})
298	−9.240		
308	−9.970	13.137	74.976
318	−10.740		

Table 2 Thermodynamic parameters of TPP–PP to methyl blue

Temperature (K)	ΔG (kJ mol^{-1})	ΔH (kJ mol^{-1})	ΔS (J mol^{-1})
298	−3.848		
308	−4.412	12.950	56.369
318	−4.975		

gas constant, the value is 8.314. Fig. 7 shows the thermodynamic adsorption curve of the TPP–PP, TPP, PP on MO solution and MB.

Using ln K_d and $1/T$ for linear regression calculation, the thermodynamic parameters can be obtained as shown in Tables 1 and 2.

At three temperatures of 25 °C, 35 °C, and 45 °C, the adsorption effect of TPP–PP on MO and MB increases as the temperature increases, and the increase in temperature helps to increase the diffusion and diffusion rate in the adsorbent.[50–52] In the thermodynamic parameters, the results show that the adsorption reaction is a spontaneous heat absorption and entropy increase reaction process, the same as the adsorption capacity and adsorption isotherm with temperature (Fig. 8 and 9).

3.6. Research on the reusability of TPP–PP

Recycling of adsorbents is a necessary condition for reducing processing costs and practical applications. In the study of the adsorption process of TPP–PP on MO, it was found that after the dye is adsorbed, 0.1 mol L^{-1} nitric acid and deionized water are used to make the adsorbed TPP–N desorption, then drying,

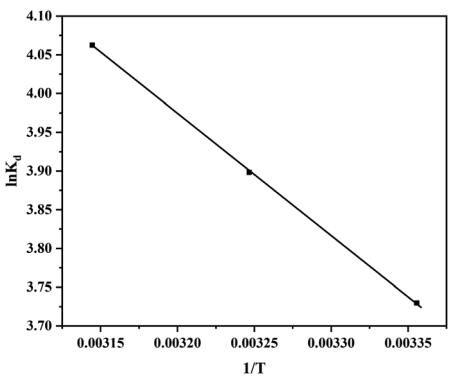

Fig. 8 Thermodynamic curve of TPP–PP adsorption of methyl orange and linear regression graph of ln K_d and $1/T$.

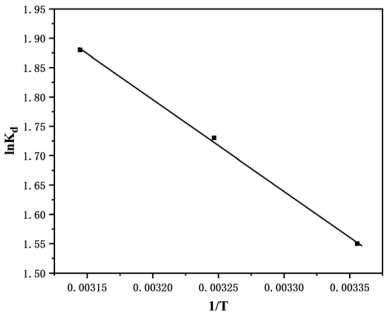

Fig. 9 Thermodynamic curve of TPP–PP adsorption of methyl blue and linear regression graph of ln K_d and $1/T$.

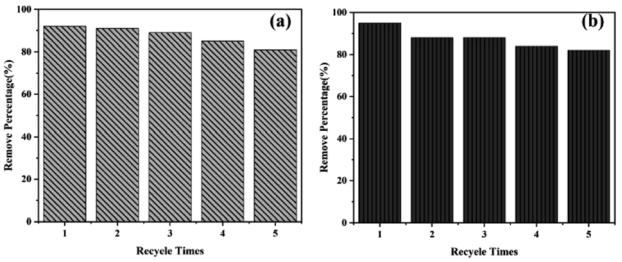

Fig. 10 (a) and (b) are the TPP–PP reusability of MO and MB.

repeat the operation 4 times. We can see from Fig. 10 that after 5 adsorption–desorption cycles, the removal performance of TPP–PP to MO and MB decreases slightly with the increase of the number of cycles, but it can still maintain more than 85% removal rate, which indicates that TPP–PP has good stability and reusability, and can effectively remove methyl orange dye and methyl blue dye from aqueous solution.

4. Conclusion

This work has the following conclusions. In this work, a new type of functionalized triptycene-based super-crosslinked porous polymer (TPP–PP) was synthesized by Friedel–Craft reaction using monomer triptycene and pyrrole as raw materials. The adsorption performance of TPP–PP was compared with triptycene porous polymer (TPP) and pyrrole polymer (PP). When the pH value of the orange solution and the methyl blue solution is 6, the maximum adsorption capacity of TPP–PP on the methyl orange solution can reach 220.82 mg g^{-1}, the maximum adsorption capacity of methyl blue solution can reach 159.8 mg g^{-1}. After 5 adsorption–desorption cycles, TPP–PP can still maintain a high removal rate. By comparison, it is found that TPP–PP has a good effect on removing MO and MB in the aqueous solution, and the adsorption performance is much better than that of TPP and PP. In summary, TPP–PP has excellent adsorption performance for the treatment of dye wastewater, and can be used as an ideal, efficient, easy to prepare, and recyclable new material for the treatment of dye wastewater.

Conflicts of interest

The authors declare no competing financial interest.

Acknowledgements

Financial support for this work was provided by the National Science Foundation of China (21908022), the Jiangxi Provincial Natural Science Foundation (20202BAB213009), Jiangxi Provincial Key Innovation Project (202110405013), and the Scientific and Technical Project of the Educational Department in Jiangxi Province (GJJ18040303).

References

1 M. E. Karim, K. Dhar and M. T. Hossain, Decolorization of Textile Reactive Dyes by Bacterial Monoculture and Consortium Screened from Textile Dyeing Effluent, *J. Genet. Eng. Biotechnol.*, 2018, **16**(2), 375–380.

2 L. Cheng, H. Yan, Z. Li, *et al.*, Fast adsorption of methylene blue, basic fuchsin, and malachite green by a novel sulfonic-grafted triptycene-based porous organic polymer, *RSC Adv.*, 2018, **8**, 41986–41993.

3 A. Rafiq, M. Ikram, S. Ali, *et al.*, Photocatalytic degradation of dyes using semiconductor photocatalysts to clean industrial water pollution, *J. Ind. Eng. Chem.*, 2021, **97**, 111–128.

4 M. R. Abhilash, G. Akshatha and S. Srikantaswamy, Photocatalytic dye degradation and biological activities of the Fe_2O_3/Cu_2O nanocomposite, *RSC Adv.*, 2019, **9**, 8557–8568.

5 P. V. Nidheesh, M. Zhou and M. A. Oturan, An overview on the removal of synthetic dyes from water by electrochemical advanced oxidation processes, *Chemosphere*, 2018, **197**, 210–227.

6 Y. Zhou, J. Lu, Y. Zhou, *et al.*, Recent advances for dyes removal using novel adsorbents: A review, *Environ. Pollut.*, 2019, **252**, 352–365.

7 Y. Wu, M. Zhang, H. Zhao, *et al.*, Functionalized mesoporous silica material and anionic dye adsorption: MCM-41 incorporated with amine groups for competitive adsorption of Acid Fuchsine and Acid Orange II, *RSC Adv.*, 2014, **4**(106), 61256–61267.

8 E. Okoniewska, Removal of Selected Dyes on Activated Carbons, *Sustainability*, 2021, **13**(8), 4300–4313.

9 B. C. Mascarenhas, F. A. Tavares and E. C. Paris, Functionalized faujasite zeolite immobilized on poly(lactic acid) composite fibers to remove dyes from aqueous media, *J. Appl. Polym. Sci.*, 2019, 48561–48573.

10 H. Sui, H. Liu, P. An, *et al.*, Application of silica gel in removing high concentrations toluene vapor by adsorption and desorption process, *J. Taiwan Inst. Chem. Eng.*, 2017, **74**, 218–224.

11 W. D. Zabka, T. Musso, M. Mosberger, *et al.*, Comparative Study of the Different Anchoring of Organometallic Dyes on Ultrathin Alumina, *J. Phys. Chem. C*, 2019, **123**(36), 22250–22260.

12 I. Shittu, A. A. Edathil, A. Alsaeedi, *et al.*, Development of novel surfactant functionalized porous graphitic carbon as an efficient adsorbent for the removal of methylene blue dye from aqueous solutions, *J. Water Process Eng.*, 2019, **28**, 69–81.

13 X. Wang, Z. Li, X. Han, *et al.*, Highly tunable porous organic polymer (POP) supports for metallocene-based ethylene polymerization, *Appl. Surf. Sci.*, 2017, **420**(1), 496–503.

14 P. Kumar, A. Das and B. Maji, Phosphorus Containing Porous Organic Polymers: Synthetic Techniques and Applications in Organic Synthesis and Catalysis, *Org. Biomol. Chem.*, 2021, **19**, 4174–4192.

15 M. G. Rabbani and H. M. El-Kaderi, Synthesis and Characterization of Porous Benzimidazole-Linked Polymers and Their Performance in Small Gas Storage and Selective Uptake, *Chem. Mater.*, 2012, **24**(8), 1511–1517.

16 T. Skorjanc, D. Shetty and M. Valant, Covalent Organic Polymers and Frameworks for Fluorescence-Based Sensors, *ACS Sens.*, 2021, **6**(4), 1461–1481.

17 X. Liu, C. Liu, W. Lai and W. Huang, Porous Organic Polymers as Promising Electrode Materials for Energy Storage Devices, *Adv. Mater. Technol.*, 2020, **5**, 2000154–2000174.

18 Z. Dong, Y. Peng, X. Zhang, *et al.*, Plasma assisted milling treatment for improving mechanical and electrical properties of *in situ* grown graphene/copper composites, *Compos. Commun.*, 2021, **24**, 100619.

19 Y. He, X. Fu, H. Wu, *et al.*, Highly efficient removal of methyl blue from aqueous solution using a novel nitrogen-doped porous magnetic carbon, *Desalin. Water Treat.*, 2020, **173**(9), 409–419.

20 V. K. Gupta and Suhas, Application of low-cost adsorbents for dye removal–a review, *J. Environ. Manage.*, 2009, **90**(8), 2313–2342.

21 L. Huang, S. Qin and S. Hu, Tannin-based magnetic porous organic polymers as robust scavengers for methylene blue and lead ions, *J. Cleaner Prod.*, 2019, **215**, 280–289.

22 S. Hou, S. Razzaque and B. Tan, Effects of synthesis methodology on microporous organic hyper-cross-linked polymers with respect to structural porosity, gas uptake performance and fluorescence properties, *Polym. Chem.*, 2019, 1299–1311.

23 Z. A. Qiao, S. H. Chai, K. Nelson, *et al.*, Polymeric molecular sieve membranes *via in situ* cross-linking of non-porous polymer membrane templates, *Nat. Commun.*, 2014, **5**, 3705–3713.

24 F. Qiu, J. Wang, D. Zhao, *et al.*, Adsorption of myo -inositol hexakisphosphate in water using recycled water treatment residual, *Environ. Sci. Pollut. Res.*, 2018, **25**(29), 29593–29604.

25 M. Haji, J. Gonzalez, J. Drysdale, *et al.*, The effects of protective shell enclosures on uranium adsorbing polymers, *Ind. Eng. Chem. Res.*, 2018, **57**, 15534–15541.

26 H. Belarbi, Philippe, *et al.*, Comparison of the benzene sorption properties of metal organic frameworks: influence of the textural properties, *Environ. Sci.: Processes Impacts*, 2019, **21**, 407–412.

27 S. Lu, Y. Hu, S. Wan, *et al.*, Synthesis of Ultrafine and Highly Dispersed Metal Nanoparticles Confined in a Thioether-Containing Covalent Organic Framework and Their Catalytic Applications, *J. Am. Chem. Soc.*, 2017, **139**(47), 17082–17088.

28 K. G. Pavithra, P. S. Kumar, V. Jaikumar, *et al.*, Removal of Colorants from Wastewater: A Review on Sources and Treatment Strategies, *J. Ind. Eng. Chem.*, 2019, **75**, 1–19.

29 X. Xu, H. Zhang, J. Ao, *et al.*, 3D hierarchical porous amidoxime fibers speed up uranium extraction from seawater, *Energy Environ. Sci.*, 2019, **12**, 1979–1988.

30 M. Babazadeh, H. Abolghasemi, M. Esmaeili, *et al.*, Comprehensive batch and continuous methyl orange removal studies using surfactant modified chitosan-clinoptilolite composite, *Sep. Purif. Technol.*, 2021, **267**(9), 118601.

31 M. Muneeb, B. Ismail, T. Fazal, *et al.*, Water treatment by photodegradation on orthorhombic antimony sulfide powder and effect of key operational parameters using methyl orange as a model pollutant, *Arabian J. Chem.*, 2015, 1117–1125.

32 B. R. Saifutdinov, V. A. Davankov, M. M. Il'In, *et al.*, Laws of sorption of some aromatic heterocycles from solutions on nanoporous supercrosslinked polystyrene, *Russ. J. Phys. Chem. A*, 2010, **84**(9), 1598–1604.

33 S. Das, T. Ben and S. Qiu, Shaping of Porous Polymers, *Polymer*, 2020, 122928.

34 Y. Luo, B. Li, W. Wang, *et al.*, Hypercrosslinked Aromatic Heterocyclic Microporous Polymers: A New Class of Highly Selective CO_2 Capturing Materials, *Adv. Mater.*, 2012, **24**(42), 5703–5707.

35 Y. Wan, Z. Y. Liu, P. Song, *et al.*, Ionic liquid groups modified 3D porous cellulose microspheres for selective adsorption of AO7 dye, *J. Cleaner Prod.*, 2019, **240**, 118201.

36 J. Kbl, D. Wechsler, E. Y. Kataev, *et al.*, Adsorption of Phenylphosphonic Acid on Rutile TiO_2(110), *Surf. Sci.*, 2020, **698**, 121612.

37 H. Yan, X. Ting, J. Hu, C. Peng, *et al.*, Amine functionalized 3D porous organic polymer as an effective adsorbent for removing organic dyes and solvents, *RSC Adv.*, 2017, **7**, 30500–30505.

38 I. S. Elizarova and P. F. Luckham, Layer-by-layer adsorption: Factors affecting the choice of substrates and polymers, *Adv. Colloid Interface Sci.*, 2018, **262**, 1–20.

39 V. Katheresan, J. Kansedo and S. Y. Lau, Efficiency of Various Recent Wastewater Dye Removal Methods: A Review, *J. Environ. Chem. Eng.*, 2018, **6**, 4676–4697.

40 S. Lu, Y. Hu, S. Wan, *et al.*, Synthesis of Ultrafine and Highly Dispersed Metal Nanoparticles Confined in a Thioether-Containing Covalent Organic Framework and Their Catalytic Applications, *J. Am. Chem. Soc.*, 2017, **139**, 17082–17088.

41 Y. A. J. Al-Hamadani, B. M. Jun, M. Yoon, *et al.*, Applications of MXene-based membranes in water purification: A review, *Chemosphere*, 2020, **254**, 126821.

42 L. Zhang, L. Sellaoui, D. Franco, *et al.*, Adsorption of dyes brilliant blue, sunset yellow and tartrazine from aqueous solution on chitosan: Analytical interpretation *via* multilayer statistical physics model, *Chem. Eng. J.*, 2020, **382**, 122952.

43 W. Li, C. Xiong, L. Wang, *et al.*, Triptycene-based porous polymers regulated by diarylethenes, *Dyes Pigm.*, 2018, **159**, 72–76.

44 S. Salvestrini, A modification of the Langmuir rate equation for diffusion-controlled adsorption kinetics, *React. Kinet., Mech. Catal.*, 2019, **128**, 571–586.

45 C. Yao and T. Chen, A film-diffusion-based adsorption kinetic equation and its application, *Chem. Eng. Res. Des.*, 2017, **119**, 87–92.

46 R. M. Mohamed, D. Mckinney, M. W. Kadi, *et al.*, Platinum/zinc oxide nanoparticles: Enhanced photocatalysts degrade malachite green dye under visible light conditions, *Ceram. Int.*, 2016, 9375–9381.

47 C. Kenyó, D. Andrea Kajtár, K. Renner, *et al.*, Functional packaging materials: factors affecting the capacity and rate of water adsorption in desiccant composites, *J. Polym. Res.*, 2013, **20**, 2–8.

48 S. Lombardo and W. Thielemans, Thermodynamics of adsorption on nanocellulose surfaces, *Cellulose*, 2019, **26**, 249–279.

49 F. Q. Ma, Y. Gui, P. Liu, *et al.*, Functional fibrous materials-based adsorbents for uranium adsorption and environmental remediation, *Chem. Eng. J.*, 2020, **390**, 124597.

50 D. Zhao, X. H. Liu, J. H. Guo, *et al.*, Porous Metal–Organic Frameworks with Chelating Multiamine Sites for Selective Adsorption and Chemical Conversion of Carbon Dioxide, *Inorg. Chem.*, 2018, **57**, 2695–2704.

51 R. Afonso, L. Gales and A. Mendes, Kinetic derivation of common isotherm equations for surface and micropore adsorption, *Adsorption*, 2016, **22**(7), 1–9.

52 E. Torrik, M. Soleimani and M. T. Ravanchi, Application of Kinetic Models for Heavy Metal Adsorption in the Single and Multicomponent Adsorption System, *Int. J. Environ. Res.*, 2019, **13**(5), 813–828.